Crystal structure of GGA2 VHS domain and its implication in plasticity in the ligand binding pocket

Guangyu Zhu[a], Xiangyuan He[b], Peng Zhai[a], Simon Terzyan[a], Jordan Tang[b], Xuejun C. Zhang[a,*]

[a] *Crystallography Research Program of Oklahoma Medical Research Foundation, 825 N.E. 13th Street, Oklahoma City, OK 73104, USA*
[b] *Protein Studies Program of Oklahoma Medical Research Foundation, 825 N.E. 13th Street, Oklahoma City, OK 73104, USA*

Received 13 December 2002; accepted 10 January 2003

First published online 7 February 2003

Edited by Irmgard Sinning

Abstract Golgi-localized, γ-ear-containing, ARF binding (GGA) proteins regulate intracellular vesicle transport by recognizing sorting signals on the cargo surface in the initial step of the budding process. The VHS (VPS27, Hrs, and STAM) domain of GGA binds with the signal peptides. Here, a crystal structure of the VHS domain of GGA2 is reported at 2.2 Å resolution, which permits a direct comparison with that of homologous proteins, GGA1 and GGA3. Significant structural difference is present in the loop between helices 6 and 7, which forms part of the ligand binding pocket. Intrinsic fluorescence spectroscopic study indicates that this loop undergoes a conformational change upon ligand binding. Thus, the current structure suggests that a conformational change induced by ligand binding occurs in this part of the ligand pocket.

Key words: VPS27, Hrs, and STAM domain; Golgi-localized γ-ear-containing ARF binding protein; Ligand binding; Crystal structure; Intrinsic fluorescence spectroscopy

1. Introduction

Cellular transport of proteins along the secretory and endocytic pathways requires the recognition and capturing of the cargo proteins by the transport carrier vesicles. It has recently become clear that a family of GGA (Golgi-localized, γ-ear-containing, ARF binding) proteins is involved in the recognition mechanism [1]. The best understood example is that of several membrane-associated receptors involved in the vesicular transport from *trans*-Golgi network (TGN) to endosomes/lysosomes, including mannose-6-phosphate receptors (MPRs) [2–4], sortilin [4,5] and the low-density lipoprotein-related protein-3 [5]. In TGN, the lumenal ends of MPRs bind the mannose-6-phosphate group on newly synthesized lysosomal hydrolases and mediate their transport to endosomes and ultimately to lysosomes; the cytosolic domain of an MPR contains sorting signals that bind members of the GGA family [2,3,5]. Three GGAs have been identified in human (GGA1–3) and two in yeast (Gga1p and Gga2p) [6–12]. They all contain four distinct domains each with specific functions. At the N-terminus, the VHS (VPS27, Hrs, and STAM) domain binds the sorting signals of receptors such as MPRs. This interaction is the recognition step in vesicle assembly. The second domain, GAT/GGAH, interacts with the GTP-bound form of ADP-ribosylation factors (ARF) [13], followed by a hinge domain containing clathrin binding motifs. At the C-terminus, the GAE/AGEH domain interacts with γ-synergin, rabaptin-5 and other potential regulators of vesicle coat assembly [6,9]. The importance of the GGA involvement in transport is illustrated by the observation that yeast with GGA gene deletion is defective in the sorting of hydrolases to its vacuoles [6,14]. Although a number of other VHS-containing multidomain proteins are known [15], they do not interact with those receptors recognized by GGAs [2]. On the ligand side, the determinant of such specificity is located in an acidic cluster-dileucine (ACDL) motif in the cytosolic region of MPRs [3]. In mammalian cells, mutations in the ACDL motif result in hypersecretion of the lysosomal enzymes [16]. The structural basis of this protein–protein interaction specificity has been illustrated by recent crystallographic studies on GGA1 and GGA3 VHS domains complexed with ligand peptides [17,18].

Recently, it has been demonstrated that an ACDL motif in the cytosolic C-terminus of memapsin-2 binds with the VHS domains of GGA1, GGA2 [19], and GGA3 (X. He and J. Tang, unpublished result). As a β-secretase, memapsin-2 is also known to initiate the cleavage of β-amyloid precursor protein leading to the production of β-amyloid peptide and the pathogenesis of Alzheimer's disease [20]. The possibility that GGA–memapsin-2 interaction may be directly involved in the intracellular transport of memapsin-2 further enhanced the importance in understanding the structural basis of interaction between VHS and signal peptides containing the ACDL motif. Here, we report a crystal structure of the human GGA2 VHS domain, which contains similar features as published for GGA1 and GGA3 [17,18]. The current structure also suggests that a ligand-induced conformational change may be involved in the binding of the ACDL signal.

*Corresponding author. Fax: (1)-405-271 7953.
E-mail address: zhangc@omrf.ouhsc.edu (X.C. Zhang).

Abbreviations: GGA, Golgi-localized, γ-ear-containing, ARF binding protein; VHS, VPS27, Hrs, and STAM domain; TGN, *trans*-Golgi network; MPR, mannose-6-phosphate receptor; ACDL, acidic cluster-dileucine; WT, wild-type; CI-MPR, cation-independent-MPR; rmsd, root mean square deviation

0014-5793/03/$22.00 © 2003 Published by Elsevier Science B.V. on behalf of the Federation of European Biochemical Societies.
doi:10.1016/S0014-5793(03)00095-4

2. Materials and methods

2.1. Protein expression and purification

The construct of glutathione-S-transferase (GST) wild-type (WT) VHS/GGA2 fusion protein has been described before [19]. The recombinant VHS protein was separated from gel-immobilized GST after thrombin cleavage, and was further purified with Resource Q ion-exchange chromatography (Amersham Biosciences, Piscataway, NJ, USA). The eluted VHS/GGA2 domain was dialyzed against a buffer of 20 mM Tris–HCl (pH 8.5) and 0.1% (v/v) β-mercaptoethanol, concentrated to 8 mg/ml and stored on ice. A VHS/GGA2 mutant of a Trp^{122} to Arg substitution (W122R) was constructed by site-directed mutagenesis using the polymerase chain reaction method, and purified as the WT recombinant protein. The mutation was confirmed by DNA sequencing. Similarly, we purified recombinant proteins of VHS/GGA1 and VHS/GGA3, which consist of residues 1–157 of both human GGA1 (GeneBank accession number AF233521) and GGA3 (AF219138).

2.2. Crystallographic study

The WT VHS/GGA2 crystal was grown at 20°C using the hanging drop method. Protein solution was mixed 1:1 (v/v) with a precipitant solution of 10% (w/v) polyethylene glycol MW 3350 (PEG3350), 5% isopropanol and 0.1 M HEPES (pH 7.5), and centrifuged to remove immediate precipitate. The supernatant was used to set 5 μl hanging drops over 500 μl reservoir solution containing 20% (w/v) PEG3350, 5% isopropanol, 0.1 M HEPES (pH 7.5), and 0.1% (v/v) β-mercaptoethanol. Crystals appeared in one day and grew to $\sim 0.2\times0.2\times0.3$ mm in size in one week. The same reservoir solution, with the addition of 20% (v/v) glycerol, was used as a cryoprotection solution to soak the crystals before being cooled in a 100 K nitrogen gas stream for data collection. X-ray diffraction data were collected from a MAR345 image plate (Mar Research Inc., Norderstedt, Germany) and Riguku X-ray generator (Molecular Structure Co., Woodlands, TX, USA) equipped with an Osmic mirror system (Osmic Inc., Troy, NI, USA), and processed with the program suite *HKL* [21]. Phases of the crystal structure were determined using the molecular replacement method with the program *AMoRe* [22]. Model building was carried out with the program *Turbo-Frodo* [23], and refinement with the program suite *CNS* [24]. No NCS restrain was applied between the two VHS molecules in an asymmetric unit during the entire refinement. Coordinates of this VHS structure have been deposited to the Protein Data Bank under the code 1mhq.

2.3. Fluorescent spectroscopic study

C-terminal peptide of cation-independent (CI)-MPR of the sequence CLVFHDDSDEDLLHI was synthesized (Synpep, Dublin, CA, USA) and purified with high-performance liquid chromatography (HPLC). Samples of VHS/GGA1–3 and the VHS^{W122R}/GGA2 were dialyzed and diluted to 0.5 μM with a buffer of 50 mM Tris–HCl (pH 7.8) and 0.1 M NaCl, in the absence and presence of 5 μM of the C-terminal peptide of CI-MPR as the ligand. Fluorescence emission spectra were recorded with an SLM Aminca Bowman-2 luminescence spectrophotometer. The excitation wavelength was 290 nm, and emission data between 300 and 400 nm were collected at 22°C. The background emission spectra of the buffer, in the absence and presence of the ligand peptide, were negligible. The wavelengths of emission maxima were determined using software provided with the instrument.

2.4. Isothermal titration calorimetry

VHS/GGA2 WT and W122R mutant samples were dialyzed into phosphate-buffered saline (PBS) (pH 7.4) with 1 mM dithiothreitol (DTT), and their concentrations were adjusted to 50 μM. The CI-MPR ligand peptide was dissolved in the same buffer to 1 mM. Titration calorimetric measurements were performed using a VP-ITC micro-calorimeter (MicroCal Inc., Northampton, MA, USA) at 30°C. The peptide ligand was injected into the VHS solution (1.4 ml) in 30 aliquots of 5 μl each. Control data, obtained from a peptide injection into a blank buffer (i.e. without VHS), were subtracted from the corresponding experimental data before being analyzed. Equilibrium dissociation constant (K_D) was determined using the computer software Origin-5.1. The stoichiometry for both WT and W122R mutant of VHS/GGA2 towards the CI-MPR ligand was determined to be 1:1.

Table 1
Crystallography data collection and refinement statistics

(a) Data statistics	
Space group	$P2_12_12_1$
Unit cell (Å) *a*	62.9
b	68.1
c	74.2
Resolution (Å)	50 (2.28)[a]−2.2
R_{merge} (%)	8.5 (44)[a]
No. of reflections	16016 (1214)[a]
Completeness (%)	95.5 (74.7)[a]
Redundancy	5.2
$I/\sigma(I)$	17.5 (2.9)[a]
(b) Refinement statistics	
$R_{working}$ (%)/no. of reflections[b]	22.3/14380
R_{free} (%)/no. of reflections[b]	26.7/737
No. of non-hydrogen atoms	
Protein	2331
Solvent	104
rmsd from ideal values	
Bond length (Å)	0.010
Bond angle (°)	1.43
Average B-factor (Å^2)	
Protein	45.9 (35.3)[c]
Solvent	48.8

[a]Numbers in parentheses are the corresponding numbers for the highest resolution shell.
[b]Reflections of $|F_{obs}| > 0.0$.
[c]The number in parentheses is the Wilson B-factor.

3. Results and discussion

3.1. Overall structure of VHS/GGA2

Based on sequence analysis [1] and structural studies of homologous GGA VHS domains [17,18], we designed a recombinant VHS/GGA2 protein consisting of residues 13–172 of the native human GGA2 [6]. The removal of the N-terminal 12 hydrophobic residues from the VHS/GGA2 construct appeared beneficial for the crystallization, since a VHS construct without the truncation failed to crystallize. The VHS/GGA2 crystal structure was determined at 2.2 Å resolution in a $P2_12_12_1$ crystal form using the molecular replacement method. There were two VHS molecules, denoted A and B, in an asymmetric unit. The following residues were excluded from the final refined model due to the absence of interpretable electron density: 12 residues at the N-terminus (i.e. residues 13–24) in both molecules, five residues of molecule A and two of B at the C-terminus, and residues 117 and 118 in molecule B. The statistics of data collection and refinement are shown in Table 1.

The overall structure of VHS/GGA2 domain was very close to those of GGA1 and GGA3 [17,18], as expected from the close sequence homology among the GGA members. The VHS/GGA2 domain contained a right-handed superhelix of eight helices (α1–α8) and a C-terminal tail of more than 10 residues, which cross-covered the helix α7 (Fig. 1). The eight α-helices could be divided into two layers: (1) α1, α3, α6 and α8, (2) α2, α4 and α7, with a two-turn helix α5 as a linker. The C_α atom root mean square deviation (rmsd) between a VHS/GGA2 monomer and those of GGA1 (PDB codes: 1jwf, 1jwg) or GGA3 (1juq, 1jpl) was in the range of 0.8–1.1 Å (using a 3 Å cutoff). Like in GGA1 [18], but unlike in VHS/GGA3 crystal structures [17], an intramolecular disulfide bond was observed between Cys^{40} and Cys^{89} in each of the two VHS/GGA2 molecules which locked helices α2 and α4, thus presumably stabilizing the overall folding.

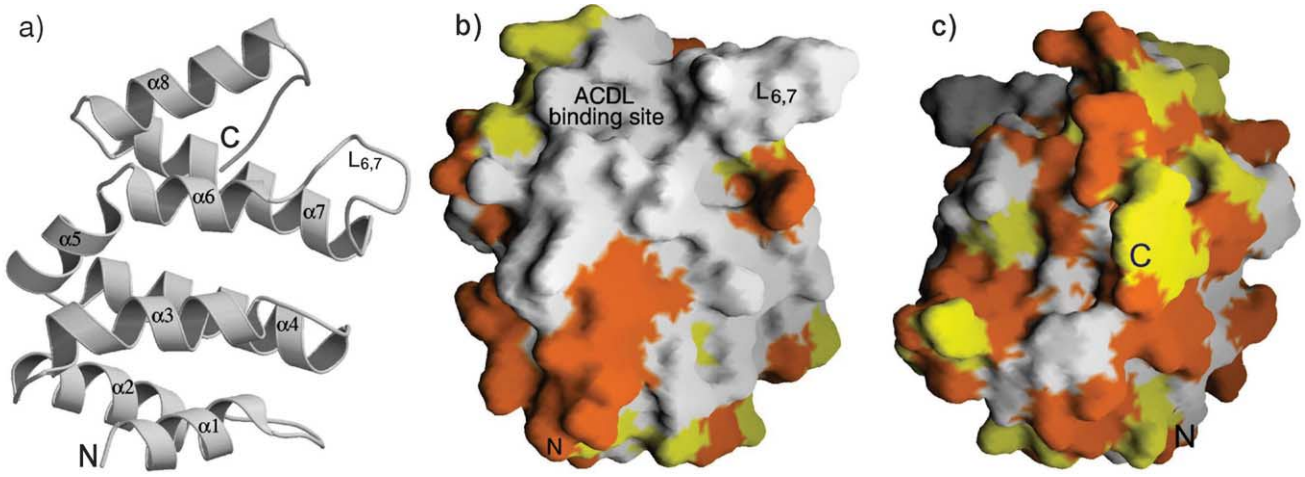

Fig. 1. Crystal structure of GGA2 VHS domain. a: A ribbon diagram with helices α1–α8 and the visible amino (N)- and carboxyl (C)-termini labeled. b: A molecular surface model in an orientation similar to a. Color coded are the amino acid residue conserveness of GGA2 compared with GGA1 and GGA3: white for identical to both, green for identical to either GGA1 or GGA3, and orange for different from both. c: The same as b but with a 180° rotation about the vertical axis. The ligand ACDL binding site, $L_{6,7}$ loop and visible N- and C-termini are labeled. This figure and Fig. 2 were drawn with programs *MolScript*, *Raster3D* or *Grasp* [27–29].

Structures of the two VHS/GGA2 molecules in the asymmetric unit were essentially identical except at the C-terminus and in a surface loop between helices α6 and α7 ($L_{6,7}$, residues 115–124). Compared to the overall 0.9 Å C_α rmsd for the majority residues (137 residues, with a 3 Å cutoff), the C-tails (residue 166 and beyond) differed by 3–6 Å between the two VHS molecules and became mobile at the tip; conformations of the visible part of C-tails appeared influenced by crystal packing. Unlike in both GGA1 and GGA3 VHS crystal structures, where the $L_{6,7}$ loop assumes a well defined helix-like conformation [17,18], this loop in GGA2 was mobile (in molecule B) and appeared to have a more extended conformation with one type-II turn [25] in the region of $K^{117}YLG^{120}$ (Fig. 2) when stabilized by the crystal packing (in molecule A). The average B-factors of the $L_{6,7}$ backbone in molecules A and B (visible part only) were 46.7 and 58.1 $Å^2$, respectively.

3.2. Ligand binding site

In both GGA1 and GGA3 VHS domains, the binding site for the ACDL motif is located between helices α6, α8, and the above mentioned loop $L_{6,7}$ [17,18]. Residues involved in the binding are highly conserved through the GGA family [18] (see Fig. 1b). Except for loop $L_{6,7}$, the conformation of the ligand binding site in VHS/GGA2 was similar to those in

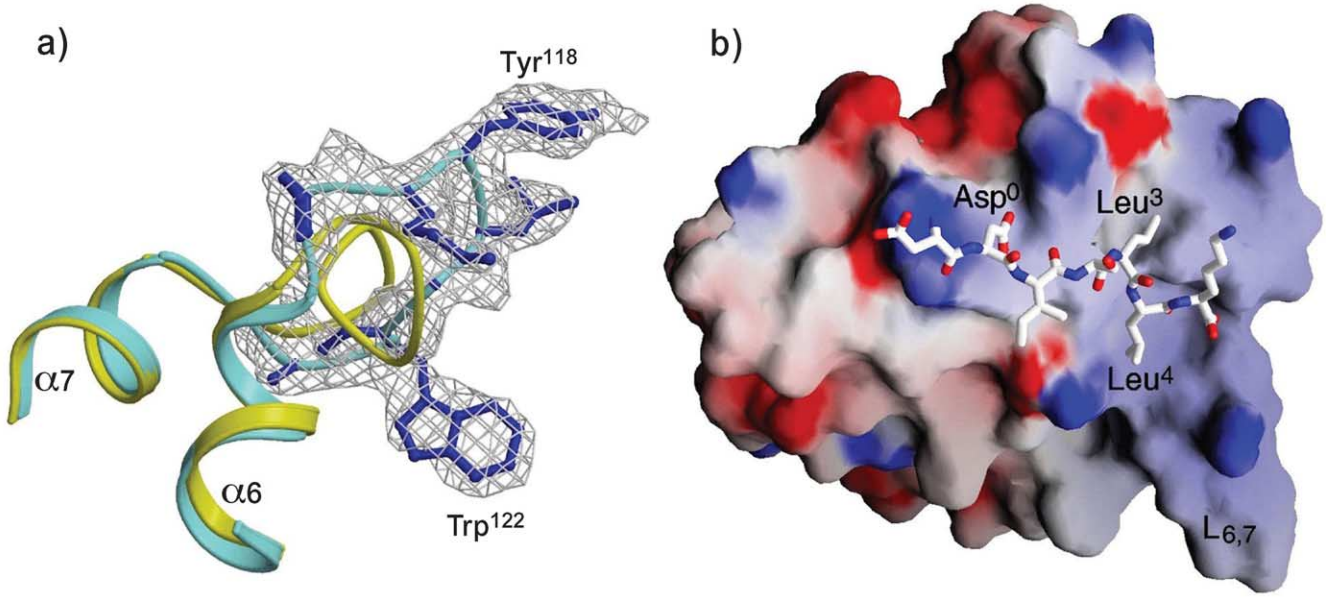

Fig. 2. Ligand binding site. a: Comparison of the $L_{6,7}$ loop region of VHS/GGA2 with that of GGA3. The C_α trace of VHS/GGA2 is shown in cyan, GGA3 (PDB code: 1jpl) in green, and side chains of $P^{116}KYLGSWA^{123}$ of GGA2 are shown in blue stick models. The corresponding portion of a $(2|F_o|-|F_c|)$ electron density map calculated with model phases is shown at 1.0σ contour level. b: Molecular modeling of memapsin-2 C-terminal peptide into the ACDL binding site of VHS/GGA2. Crystal structures of VHS/GGA1,3–ligand complexes [17,18] were used as the template. The memapsin-2 C-terminal peptide (of sequence $DD^0ISL^3L^4K$) is shown in stick models (oxygen atoms in red, nitrogen in blue, and carbon in white). VHS domain is shown in a molecular surface model, where the color intensity corresponds to the calculated electrostatic potential, from −8 kT/e (intense red) to +8 kT/e (intense blue).

GGA1 and GGA3. Not surprisingly, the conformations of the side chains of residues in this putative ligand binding site of GGA2 were more similar to those in the ligand-free form of VHS/GGA1 crystal than to the ligand-bound forms. For example, both χ_1 angles of Phe[104] and Asn[108] assumed a *trans* rotamer in ligand-free VHS domains of GGA1 and GGA2, but switched to a g^+ rotamer in the crystal structures of VHS/GGA1 and VHS/GGA3 complexed with an MPR C-terminal peptide. On the other hand, given the current VHS/GGA2 structure containing a more extended conformation at loop $L_{6,7}$, some of the ligand-interacting residues seen in VHS/GGA1 and VHS/GGA3 would not be in positions to interact with ligand ACDL in VHS/GGA2. For example, a Lys[117] equivalent (Lys[100] in molecule B of PDB file 1juq) was observed being involved in an electrostatic interaction with the carboxyl-terminal group of the peptide ligand, and the hydroxyl group of Tyr[118] equivalents (Tyr[101] in molecules B and D of 1juq, and Tyr[102] in molecule A of 1jwg) formed a hydrogen bond with a peptide carbonyl oxygen of the ligand. With the more open conformation observed in VHS/GGA2, the two residues would not be in positions to interact with the peptide unless the loop $L_{6,7}$ changes its conformation upon peptide binding.

3.3. VHS dimer in crystal

In a crystallographic asymmetric unit, the two VHS/GGA2 molecules formed a symmetric dimer with the dyad axis in a general orientation in the orthorhombic crystal lattice (i.e. 23° off the *X*–*Z* plane and 55° away from the *Z* axis). The dyad axis was roughly parallel to the surface plane formed by helices α1, α3, and α6, perpendicular to their helix axes. Around 1560 Å^2 (i.e. ~10%) solvent accessible surface from the two VHS molecules was buried in the dimer interface, which was formed mainly with the helices α1 and α3 and their following loops. Most of the residues involved in the interface are conserved among GGAs, but are variable in other VHS-containing proteins. The side chain imidazole rings of the two His[69] residues stacked together forming the center piece of the dimer interface and were sandwiched by Pro[74] residues from both sides. Asn[31] and Gln[75] formed two pairs of intermolecular hydrogen bonds. In addition, there were several water-bridged hydrogen bonds within the interface. It is structurally interesting to notice that the same dimerization has repeatedly appeared in other GGA VHS crystal forms obtained under varied crystallization conditions (see PDB files 1jwg, 1juq, and 1jpl). However, consistent with previous observations that GGA VHS domains stay as monomers in solution [17], we could not detect dimerization of VHS/GGA2 in a pull-down assay (data not shown).

3.4. Loop $L_{6,7}$ changes its conformation upon binding a ligand

The structural observation that the loop $L_{6,7}$ assumes different conformations between the apo- and ligand-bound forms of GGA VHS crystal structures prompted us to hypothesize that this loop changes its conformation upon ligand binding. To test this, we performed an intrinsic fluorescence spectroscopic study on the VHS/GGA2 domain in both absence and presence of a ligand peptide. This experiment took advantage of Trp[122] in the loop $L_{6,7}$ of VHS/GGA2. The WT VHS/GGA2 contains six tryptophan residues (i.e. 29, 43, 65, 122, 138 and 141). None of these residues would be in direct contact with the potential ligand according to the ligand complex crystal structures of homologous proteins [17,18]. For example, in the crystal structure of CI-MPR peptide–VHS/GGA3 complex (PDB file 1jpl), the closest distance from the ligand to the side chain of Arg[105], which is the equivalent residue of VHS/GGA2 Trp[122], is over 14 Å. Therefore, the potential fluorescence probe, Trp[122], in VHS/GGA2 was more likely to detect an environmental change caused by the loop conformational change rather than directly by the ligand binding. Based on structural comparison, the Trp[122] side chain would be in a more open environment in the helical conformation than in the current structure. The C_β atom of Trp[122] in the current structure is 4.7 Å from the C_β of the nearby Pro[57] in the loop between α3 and α4; this distance becomes 6.7 Å in the projected structure of a helix-like $L_{6,7}$ loop. Therefore, the ligand-bound form was predicted to have a reduced intrinsic fluorescent signal because of solvent quenching.

Indeed, compared with the apo-form, the ligand-bound VHS/GGA2 showed a 10% decrease in the maximum fluorescent emission intensity (Fig. 3 and Table 2). To further confirm that this reduction of fluorescent signal was mainly contributed by the environmental change of Trp[122], a mutant VHS/GGA2 was constructed as a negative control by substituting Trp[122] with Arg, the latter of which is the corresponding residue in both GGA1 and GGA3. The resulting W122R mutant had an equilibrium dissociation constant (K_D 11.5 ± 0.2 μM) towards the CI-MPR ligand comparable with that of the WT (10.7 ± 0.2 μM). As predicted by our hypothesis, this mutant showed essentially no change in the fluorescent emission upon ligand binding. This result supports the notion that Trp[122] side chain in WT VHS/GGA2 is subjected to an environmental change upon ligand binding. Consistent with the lack of a tryptophan residue in their $L_{6,7}$ loop, VHS/GGA1 and VHS/GGA3 did not show significant change in the fluorescent signal upon ligand binding (see Table 2).

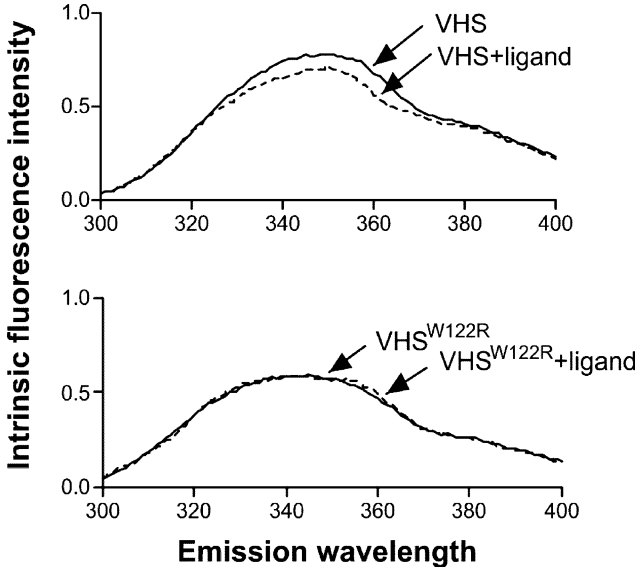

Fig. 3. Intrinsic fluorescence spectra of VHS/GGA2. Typical emission spectra of WT (top) and W122R mutant (bottom) of VHS/GGA2 in the absence (solid line) and presence (dashed line) of the CI-MPR peptide are shown, which suggest that GGA2 Trp[122] was subjected to an environmental change upon ligand binding. Fluorescence intensities are shown in an arbitrary unit.

Table 2
Effect of the binding of CI-MPR C-terminal peptide on the intrinsic fluorescence properties of GGA VHS domains

	Relative intensity (ligand-bound/apo)	Emission maxima (nm)	
		apo-protein	ligand-bound
VHS/GGA2	0.89 ± 0.02	351 ± 1	349 ± 1
VHS^{W122R}/GGA2	1.02 ± 0.01	341 ± 1	341 ± 1
VHS/GGA1	1.02 ± 0.02	339 ± 1	339 ± 1
VHS/GGA3	1.05 ± 0.02	338 ± 1	338 ± 1

Results were based on at least triplet measurements. Also see Section 2.

3.5. Structural implications

Consistent with the common function of binding the sorting signal in the cargo, GGAs share 55% sequence identity (and ~90% homology) in their VHS domains and a conserved overall three-dimensional structure [17,18]. The amino acid residue variation is mainly concentrated on the molecular surface of the helix layer formed by α2, α4 and α7 (see Fig. 1b, c), which may implicate differences of GGAs in their subsequent interactions with other proteins in the assembly. The close homology of VHS/GGAs suggests that the interaction of VHS/GGA2 with a peptide ligand can be reasonably assessed from modeling using the existing information on ligand interaction of VHS/GGA1 and VHS/GGA3. We, therefore, modeled the binding of memapsin-2 C-tail peptide to VHS/GGA2 (Fig. 2b) to illustrate that this peptide or a similar one is capable of interacting with VHS/GGA2 in a similar mode as those of GGA1 and GGA3. The structural adjustment required for this docking included mostly rotamer changes of a few side chains. Since there was no stereo collision between the ligand and VHS, no energy minimization was performed. In this preliminary model, the key residues of the ACDL motif, i.e. Asp^{0}, Leu^{3} and Leu^{4}, resided in the shallow pockets of complementary features as described before [17,18]; side chains of Ile^{1} and Ser^{2} were exposed to solvent; and the terminal carboxyl group of memapsin-2 could be stabilized by an interaction with the side chain of Gln^{158} of GGA2. However, binding of other ligands, e.g. a CI-MPR C-terminal peptide, would require further conformational adjustment in the $L_{6,7}$ loop. Compared with previously reported VHS/GGA domain crystal structures [17,18], conformation of the $L_{6,7}$ loop in VHS/GGA2 is significantly different. In all the VHS/GGA1 and VHS/GGA3 crystal structures, both with or without ligands, this loop assumes a helix-like conformation consisting of two consecutive type-I turns [25]. It directly interacts with peptide ligands of MPR C-termini in the complex crystal structures, and is considered a structural determinant for the ligand specificity. In the current VHS/GGA2 crystal structure, this loop assumes a more extended conformation with one type-II turn. The N-terminal six-residue sequence of the $L_{6,7}$ loop (i.e. S^{115}PKYLG^{120}) is identical in all GGA1–3, whereas that of the remaining four residues in the loop changes from (S/D)R(T/V)S in GGA1/3 to S^{121}WAT^{124} in GGA2. However, the backbone conformational difference between the helix-like form in GGA1/3 and the more open form in GGA2 mainly lies in the conserved region; thus, it is unlikely that the extended conformation of $L_{6,7}$ is a special structural feature of GGA2 determined by its amino acid sequence. Similar to the crystal structures of VHS domains of GGA1/3, the C-terminal part of the $L_{6,7}$ loop in VHS/GGA2 is partially involved in the homodimer interface, which precludes a possibility that the dimer formation causes the conformational difference in $L_{6,7}$. Our data, from the intrinsic tryptophan fluorescence study, support the structural interpretation that ligand binding induces a conformational change in the $L_{6,7}$ loop of VHS/GGA2. Although it has not been tested, it is interesting to note the possibility that such conformational flexibility would allow the VHS domain to accommodate ligands of different peptide length beyond the C-terminus of the ACDL motif, and to achieve different affinity for different ligands [26].

Acknowledgements: The authors thank Dr. K. Rodger of the Department of Biochemistry and Molecular Biology, University of Oklahoma Health Sciences Center, for helping with the isothermal titration calorimetry experiment. This work was in part supported by NIH grant AG-18933 and the Alzheimer's Association Pioneer Award to J.T.; and X.C.Z. was supported by NIH grant HL60626.

References

[1] Lohi, O., Poussu, A., Mao, Y., Quiocho, F. and Lehto, V.P. (2002) FEBS Lett. 513, 19–23.
[2] Puertollano, R., Aguilar, R.C., Gorshkova, I., Crouch, R.J. and Bonifacino, J.S. (2001) Science 292, 1712–1716.
[3] Zhu, Y., Doray, B., Poussu, A., Lehto, V.P. and Kornfeld, S. (2001) Science 292, 1716–1718.
[4] Takatsu, H., Katoh, Y., Shiba, Y. and Nakayama, K. (2001) J. Biol. Chem. 276, 28541–28545.
[5] Nielsen, M.S., Madsen, P., Christensen, E.I., Nykjaer, A., Gliemann, J., Kasper, D., Pohlmann, R. and Petersen, C.M. (2001) EMBO J. 20, 2180–2190.
[6] Hirst, J., Lui, W.W., Bright, N.A., Totty, N., Seaman, M.N. and Robinson, M.S. (2000) J. Cell Biol. 149, 67–80.
[7] Dell'Angelica, E.C., Puertollano, R., Mullins, C., Aguilar, R.C., Vargas, J.D., Hartnell, L.M. and Bonifacino, J.S. (2000) J. Cell Biol. 149, 81–94.
[8] Boman, A.L., Zhang, C., Zhu, X. and Kahn, R.A. (2000) Mol. Biol. Cell 11, 1241–1255.
[9] Takatsu, H., Yoshino, K. and Nakayama, K. (2000) Biochem. Biophys. Res. Commun. 271, 719–725.
[10] Black, M.W. and Pelham, H.R. (2000) J. Cell Biol. 151, 587–600.
[11] Zhdankina, O., Strand, N.L., Redmond, J.M. and Boman, A.L. (2001) Yeast 18, 1–18.
[12] Poussu, A., Lohi, O. and Lehto, V.P. (2000) J. Biol. Chem. 275, 7176–7183.
[13] Takatsu, H., Yoshino, K., Toda, K. and Nakayama, K. (2002) Biochem. J. 365, 369–378.
[14] Mullins, C. and Bonifacino, J.S. (2001) Mol. Cell. Biol. 21, 7981–7994.
[15] Lohi, O. and Lehto, V.P. (1998) FEBS Lett. 440, 255–257.
[16] Lobel, P., Fujimoto, K., Ye, R.D., Griffiths, G. and Kornfeld, S. (1989) Cell 57, 787–796.
[17] Misra, S., Puertollano, R., Kato, Y., Bonifacino, J.S. and Hurley, J.H. (2002) Nature 415, 933–937.
[18] Shiba, T. et al. (2002) Nature 415, 937–941.
[19] He, X., Chang, W.P., Koelsch, G. and Tang, J. (2002) FEBS Lett. 524, 183–187.
[20] Selkoe, D.J. and Podlisny, M.B. (2002) Annu. Rev. Genomics Hum. Genet. 3, 67–99.
[21] Otwinowski, Z. and Minor, W. (1997) Methods Enzymol. 276, 307–326.
[22] Navaza, J. (1994) Acta Crystallogr. A50, 157–163.

[23] Roussel, A. and Cambillau, C. (1989) in: Sillicon Graphics Geometry Partners Directory, pp. 77–79, Silican Graphics, Mountain View, CA.
[24] Brunger, A.T. et al. (1998) Acta Crystallogr. D Biol. Crystallogr. 54, 905–921.
[25] Richardson, J.S. (1981) Adv. Protein Chem. 34, 167–339.
[26] Doray, B., Bruns, K., Ghosh, P. and Kornfeld, S. (2002) J. Biol. Chem. 277, 18477–18482.
[27] Kraulis, P.J. (1991) J. Appl. Crystallogr. 24, 946–950.
[28] Merritt, E.A. and Murphy, M.E.P. (1994) Acta Crystallogr. D 50, 869–873.
[29] Nicholls, A., Sharp, K.A. and Honig, B. (1991) Proteins 11, 281–296.